Molecular Biology of the Cell
Vol. 19, 2026–2038, May 2008

Paralemmin-1, a Modulator of Filopodia Induction Is Required for Spine Maturation

Pamela Arstikaitis,* Catherine Gauthier-Campbell,* Rosario Carolina Gutierrez Herrera,† Kun Huang,* Joshua N. Levinson,* Timothy H. Murphy,* Manfred W. Kilimann,‡ Carlo Sala,§ Michael A. Colicos,† and Alaa El-Husseini*

*Department of Psychiatry and the Brain Research Centre, University of British Columbia, Vancouver, V6T 1Z3, Canada; §Department of Pharmacology, CNR Institute of Neuroscience, University of Milan, Milan, Italy; †Department of Physiology and Biophysics, Hotchkiss Brain Institute, University of Calgary, Calgary, T2N 4N1, Canada; and ‡Department of Cell and Molecular Biology, Uppsala University, 75124 Uppsala, Sweden

Submitted August 19, 2007; Revised January 29, 2008; Accepted February 7, 2008
Monitoring Editor: Paul Forscher

Dendritic filopodia are thought to participate in neuronal contact formation and development of dendritic spines; however, molecules that regulate filopodia extension and their maturation to spines remain largely unknown. Here we identify paralemmin-1 as a regulator of filopodia induction and spine maturation. Paralemmin-1 localizes to dendritic membranes, and its ability to induce filopodia and recruit synaptic elements to contact sites requires protein acylation. Effects of paralemmin-1 on synapse maturation are modulated by alternative splicing that regulates spine formation and recruitment of AMPA-type glutamate receptors. Paralemmin-1 enrichment at the plasma membrane is subject to rapid changes in neuronal excitability, and this process controls neuronal activity-driven effects on protrusion expansion. Knockdown of paralemmin-1 in developing neurons reduces the number of filopodia and spines formed and diminishes the effects of Shank1b on the transformation of existing filopodia into spines. Our study identifies a key role for paralemmin-1 in spine maturation through modulation of filopodia induction.

INTRODUCTION

During CNS excitatory synapse development, the formation of spines, bulbous protrusions enriched with F-actin, is essential for proper synaptic transmission and neuronal function (Hall and Nobes, 2000; Yuste and Bonhoeffer, 2004; Halpain *et al.*, 2005; Matus, 2005; Gerrow and El-Husseini, 2006). Spines contain a plethora of proteins including neurotransmitter receptors, cytoskeleton-associated proteins, and cell adhesion molecules. Spines are pleomorphic protrusions that can be modified by changes in neuronal activity, which regulate actin-based motility (Fischer *et al.*, 1998; Portera-Cailliau *et al.*, 2003; Matus, 2005). Defects in spine maturation and function have been associated with several forms of mental retardation including Down, Rett, Fragile X, and fetal alcohol syndromes. Some of these disorders exhibit a reduction in spine size and density and the formation of long, thin filopodia-like structures (Hering and Sheng, 2001; Zoghbi, 2003).

Although our knowledge of molecules that control the morphology and functional properties of dendritic spines has expanded, information about the structures from which spines emerge is lacking. Dendritic filopodia, thin protrusions ranging in length from 2 to 35 μm, are thought to participate in synaptogenesis, dendritic branching and the development of spines. During synaptogenesis, filopodia decorate the dendrites of neurons. Studies show that dendritic filopodia exhibit highly dynamic protrusive motility during periods of active synaptogenesis (Dailey and Smith, 1996; Ziv and Smith, 1996; Marrs *et al.*, 2001). Thus, filopodia are thought to function by extending and probing the environment for appropriate presynaptic partners, thereby aiding in synapse formation. These results are further supported by electron microscopy studies which show that synapses can be formed at the tip and base of dendritic filopodia (Fiala *et al.*, 1998; Kirov *et al.*, 2004). As synapses form, the number of filopodia declines and the number of spines increases, suggesting the involvement of dendritic filopodia in spine emergence (Zuo *et al.*, 2005a,b). Decreased spine density and increased density of filopodia-like protrusions associated with several brain diseases lends further support to the notion that filopodia serve as precursors to spines (Fiala *et al.*, 2002; Calabrese *et al.*, 2006). However, no direct evidence illustrating the emergence of spines from filopodia has been found. Also, the molecular machinery required for filopodia induction and transformation to spines remains unknown.

A candidate protein that regulates filopodia induction in neurons is paralemmin-1, a molecule shown to induce cell expansion and process formation. Paralemmin-1 is abundantly expressed in the brain and concentrated at sites of plasma membrane activity, where it is anchored to the plasma membrane through lipid modifications. (Burwinkel *et al.*, 1998; Kutzleb *et al.*, 1998; Gauthier-Campbell *et al.*, 2004; Castellini *et al.*, 2005; Basile *et al.*, 2006; Kutzleb *et al.*,

This article was published online ahead of print in *MBC in Press* (http://www.molbiolcell.org/cgi/doi/10.1091/mbc.E07–08–0802) on February 20, 2008.

Address correspondence to: Pamela Arstikaitis (parstika@interchange.ubc.ca).

2007). This protein localizes to the plasma membranes of postsynaptic specializations, axonal and dendritic processes, and perikarya.

Using a combination of live imaging, as well as loss- and gain-of-function approaches, our analysis identifies paralemmin-1 as a regulator of filopodia induction, synapse formation, and spine maturation. We also reveal an important role for paralemmin-1 in recruitment of AMPA-type glutamate receptors, a process governed by alternative splicing of paralemmin-1. These effects are modified by neuronal activity that induces rapid translocation of paralemmin-1 to the plasma membrane. Activity-driven translocation of paralemmin-1 to membranes results in rapid protrusion expansion, emphasizing the importance of paralemmin-1 in paradigms that control structural changes associated with synaptic plasticity and learning. Finally, we show that knockdown of paralemmin-1 results in loss of filopodia and compromises spine maturation induced by Shank1b, a protein that facilitates rapid transformation of newly formed filopodia to spines. These findings elucidate an important role for paralemmin-1 in filopodia induction and spine maturation.

MATERIALS AND METHODS

cDNA Cloning and Mutagenesis

Wild-type and cysteine mutant forms of mouse paralemmin-1 were generated by PCR and cloned in to the multiple cloning site (MCS) in pEGFP-C1 vector (Clontech, Mountain View, CA) at BglII and HindIII restriction sites. Construction of Shank1b in to a GW1 expression vector occurred as previously described (Lim *et al.,* 1999). RNA interference (RNAi) generated against identical sequences in both mouse and rat paralemmin-1 were introduced into pSUPER vector (Clontech) into the HindIII/BglII sites and contained the following sequence GAAGAAGCCTCGCTGTAGA. Scrambled RNAi (Ctl RNAi) was subcloned as previously described (Huang *et al.,* 2004). RNAi resistant paralemmin-1 was generated by creating five silent point mutations on the RNAi target sequence using the Stratagene site-directed mutagenesis kit (Stratagene. La Jolla, CA) following the manufacturer's instructions. The underlined nucleotides were mutated in the paralemmin-1 RNAi sequence GAAAAAACCACGATGCAGA. All constructs were verified by DNA sequencing.

Primary Neuronal Culture Preparation, Transfection, Treatments, and Immunocytochemistry

Neuronal cultures were prepared from hippocampal embryonic day 18/19 rats. Cells were plated at 125,000 cells per coverslip as previously described (Gerrow *et al.,* 2006). For neuronal depolarization, hippocampal neurons were treated either with 90 mM KCl for 3 min or with 50 mM KCl for 10 min during time-lapse imaging. For immunocytochemistry, COS-7 cells and hippocampal neurons were fixed with 2% paraformaldehyde and 4% sucrose or with methanol at −20°C when staining for synaptic proteins. Fixative was removed, and cells were washed three times with phosphate-buffered saline (PBS) containing 0.3% triton to permeabilize cells. The following primary antibodies were used: green fluorescent protein (GFP; chicken; 1:1000; Abcam, Cambridge, MA), GluR1 (rabbit; 1:500; Upstate Biotech, Lake Placid, NY) and hemagglutinin (HA; mouse; 1:1000; Synaptic Systems, Göttingen, Germany). For endogenous paralemmin-1 detection, rabbit anti-paralemmin-1 sera 2 and 10 were used (Kutzleb *et al.,* 1998). We used the following secondary antibodies: Alexa 488–conjugated anti-chicken (1:1000, Molecular Probes, Eugene, OR), Alexa 568–conjugated anti-mouse (1:1000, Molecular Probes), and Alexa 568–conjugated anti-rabbit (1:1000, Molecular Probes). Coverslips were incubated for 1 h at room temperature with primary and secondary antibodies. To detect filopodia in COS-7 cells, we incubated cells for 40 min with rhodamine-labeled phalloidin (Molecular Probes). Coverslips were mounted with Flouromount-G (Southern Biotechnology Associates, Birmingham, AL).

Microscopy and Time-Lapse Recordings

Fluorescent images were acquired using a 63× objective coupled (NA = 1.4) to a Zeiss Axiovert M200 motorized inverted light microscope and Axiovision software (Thornwood, NY). To correct for potentially out of focus filopodia z-projections were taken in 0.500-μm sections. Time-lapse imaging occurred in an environmentally controlled chamber with 5% carbon dioxide at 37°C as previously described (Gerrow *et al.,* 2006). Hippocampal neurons were plated on glass microwell dishes (MatTek, Ashland, MA) at a density of 400,000 cells per dish. Images were acquired every 2 min for 2–3 h. For quantification of time-lapse imaging, the total number of filopodia and spine-like protrusions were counted at time = 0 h, based on criteria under quantitative measurement of filopodia and spines and expressed as a number per 100 μm of dendritic length. Next, the fate of every protrusion counted at t = 0 h was manually tracked, traced, and recorded. The frequency of four events (spine-like to filopodia, filopodia to spine-like, stable filopodia, and stable spines) that we focused on were recorded for each cell. Finally, we have expressed the total average of an event by the total number of filopodia or spines/100 μm of dendrite.

For confocal microscopy, images were captured using the Zeiss Confocal LSM510 Meta system 63× objective (NA = 1.2) water lens as previously described (Kang *et al.,* 2004). Images were captured using a 512 × 512-pixel screen, and gain settings for both fluorophores were 600–800. Scan speed function was set to 6, and the mean of 16 lines was detected. Zoom function was set to 1 and the pinhole was set to 1 airy unit for all experiments. Z-series were used to capture out-of-focus dendrites and sections.

Analysis of Paralemmin-1 Accumulation at the Membrane

To assess changes in paralemmin-1 expression at the membrane we used the Image J program (NIH; http://rsb.info.nih.gov/ij/). Images were acquired using confocal microscopy, which allowed us to define membrane versus cytoplasm expression. Images were exported as 16 bit and analyzed using the segmented line tool. To assess changes in membrane localization of endogenous paralemmin-1 by KCl and 2-bromopalmitate (BP) treatments, the fluorescence intensity of lines drawn through the top and bottom portions of dendrites (membrane) versus the fluorescence intensity of a line drawn through the middle portion of a dendrite (cytoplasm) were contrasted. This analysis was performed in days in vitro 16–18 (DIV 16–18), at a developmental stage where hippocampal neurons possess thick dendritic segments. An average membrane and cytoplasm fluorescence was calculated for all dendrites pertaining to each neuron. Statistical analyses were performed using Excel software (Microsoft, Redmond, WA). All analyses were performed by an individual blinded to treatment conditions.

Quantification of KCl Enlargement of Dendritic Protrusions

Time-lapse imaging was performed over a 10 min interval, and images were collected every 5 min as previously described (Gerrow *et al.,* 2006). The total number of protrusions per cell was quantified before and after KCl stimulation and expressed as the number of protrusions/100 μm of dendritic length. The average diameter of protrusions, taken at the base and tips was measured. For this analysis, all protrusions (including those that did not change) on individual cells were examined and were measured before and after KCl treatment. A protrusion enlargement of greater than 2 μm was counted as an "enlarged protrusion" and expressed as a percent of change in protrusion size. For irregularly shaped protrusions, the area was measured using Northern Eclipse software (Empix Imaging, Mississauga, ON, Canada). Briefly, the entire structure (from base to the tip) before and after stimulation was manually traced, and these included growth-cone, lamellopodia-like structures, membrane expansion at the tip of filopodia, and expansion of existing protrusions. The data were further analyzed using Excel software.

Photoconductive Stimulation and Quantification

Rat hippocampal neurons taken from postnatal day 0 (P0) pups were grown on silicon wafers as previously described (Colicos *et al.,* 2001; Colicos and Syed, 2006; Goda and Colicos, 2006). Neuronal cultures were grown until DIV 4, at which time they were transfected using Lipofectamine 2000 (Invitrogen, Burlington, ON, Canada) and stimulated 3–4 d later. In brief, the cultures were transferred to serum-free media for 1.5 h and then incubated with 1.5 μg of paralemmin-L DNA. Control image sequences were acquired before stimulation, using a WAT105N (Watec, Yamagata-Ken, Japan) camera on an Olympus BX60WI microscope (Melville, NY). Neurons were then stimulated at 30 Hz for 15 s, and images were acquired every 5 s for the next 10 min. Densitometry was performed on single images from the control sequence and after stimulation using Image J software (NIH). Membrane and cytoplasm regions were selected randomly and regions of interest (ROI) were defined over a segment of the membrane, and the average pixel value was calculated. ROIs were variable in size, depending on the thickness of the dendrite analyzed. Areas in the membrane included from 1–2 pixels wide by 2–3 pixels and from 1–2 pixels wide by 3–4 pixels in length. This ROI was then moved immediately inward from the membrane, and the average pixel value was calculated. These two values were used to produce the ratio between the intensity of GFP-paralemmin-L signal inside the dendrite versus at the membrane. Ratios from multiple experiments were averaged, and the error was calculated as the SE of the ratio.

Quantitative Measurement of Filopodia and Spines

Filopodia induction in COS-7 cells was scored according to the following criteria: within a field of view, cells with three filopodia or more were counted as cells "with filopodia," and all other cells within the same field of view were counted as cells "without filopodia." Filopodia induction is expressed as percent of cells scored "with filopodia" normalized to a GFP control. For

analysis of filopodia and spines in neuronal cells, images were scaled to 16 bits and analyzed using Northern Eclipse Software (Empix Imaging) and automatically logged into Excel (Microsoft). Any protrusion ranging in length from 2 to 10 μm and lacking a visible head (<0.35 μm) was counted as "filopodia" and marked. In all of our analyses, filopodia in general, were clearly distinguishable. However, in a few instances, filopodia could appear intermingled if the density was too high and were difficult to quantify. Spines were counted separately, and spine heads were measured using the polygon tool and were only scored as a "spine-like" if a clear head greater than 0.35 μm in width was measured. Finally, for morphological measurements the entire lengths of all primary, secondary, and tertiary dendrites extending from the cell body were measured using the curve measurement tool and expressed as protrusions per unit length (100 μm) of dendrite. All analyses were performed by an individual blinded to treatment conditions.

Subcellular Fractionation

Cultured cortical neurons (DIV 16–20; 12 $\times$ 10^6 cells) were treated for 3 min with or without 90 mM KCl. Cells were washed 1$\times$ with PBS, harvested, and then suspended in 200 μl of sonication buffer (50 mM Tris, pH 7.4, 0.1 mM EGTA) supplemented with a protease inhibitor cocktail (2.5 μg/ml leupeptin, 2.5 μg/ml aprotinin, and 1 μM PMSF). Cells were sonicated on ice for 16 s, and nuclei were pelleted at 14,000 $\times$ *g* at 4°C for 10 min. Lysates were centrifuged at 49,000 $\times$ *g* for 1 h at 4°C. The supernatants were collected, and pellets were resuspended in 150 μl resuspension buffer (RB; 50 mM Tris, pH 7.4, 0.1 mM EGTA, 1 M KCl, 10% glycerol, 1.5 μl/10 ml BME, and protease inhibitors). Fractions (30 μl each) were analyzed by SDS-PAGE, and membranes were probed for paralemmin-1 and transferrin receptor. Image J software was used to quantify paralemmin-1 band intensity by plotting the peaks and a Student's paired *t* test was used to determine statistical significance.

RESULTS

Paralemmin-1 Regulates Protrusion Formation in Developing Neurons

Previous investigations identified paralemmin-1 as a candidate protein that regulates filopodia induction in heterologous cells; however, its role in neurons has not been explored (Kutzleb *et al.*, 1998). Consistent with a potential role for paralemmin-1 in filopodia induction, endogenous paralemmin-1 is detected in filopodia and spines in both immature (DIV 10) and mature (DIV 26) hippocampal neurons (Figure 1A). Alternative splicing of paralemmin-1 is developmentally regulated (Kutzleb *et al.*, 1998). The expression of a short splice variant (paralemmin-S) lacking exon 8 occurs early in development, preceding spine formation,

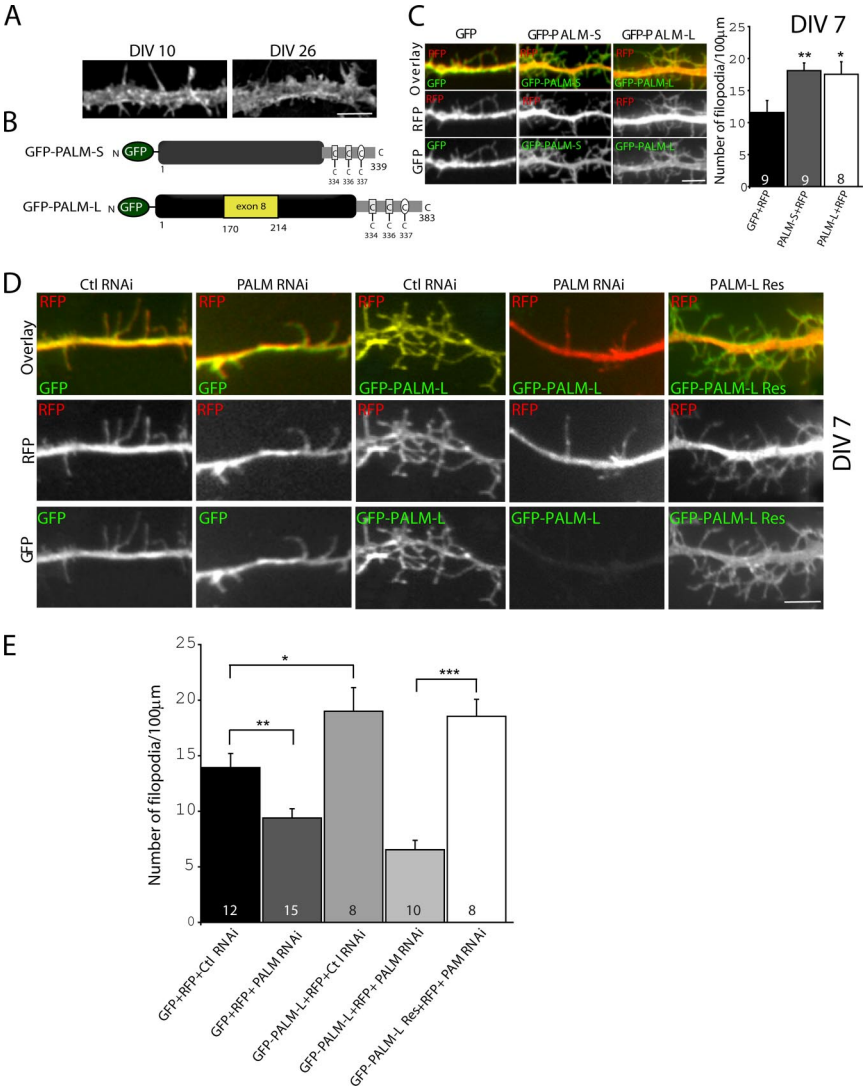

Figure 1. Paralemmin-1 is required for filopodia induction in developing neurons. (A) Paralemmin-1 is localized to the plasma membrane, filopodia, and spines in primary hippocampal neurons. Immunocytochemical staining of cultured hippocampal neurons reveals that paralemmin-1 is localized in patches along the plasma membrane. It is also detected in dendritic filopodia at 10 days in vitro (DIV 10) and spines in mature neurons (DIV26). (B) Diagram showing structure of wild-type GFP-tagged paralemmin-1 splice variants. Location of the palmitoylated cysteines (C334, C336) and the prenylated residue (C337) is indicated. (C) Both paralemmin-1 splice variants induce filopodia at DIV 7. Hippocampal neurons were cotransfected at DIV 5 with RFP and either GFP, GFP-paralemmin-S, the short variant of paralemmin-1 lacking sequences encoded by exon 8 (GFP-PALM-S) or GFP-paralemmin-L, the long variant containing sequences encoded by exon 8 (GFP-PALM-L). Quantification of the number of filopodia/100 μm shows that expression of both paralemmin-1 splice variants increase filopodia number. Number of cells analyzed for each group is indicated at the bottom of each bar. Number of filopodia analyzed per group: GFP+RFP = 270, GFP-PALM-S+RFP = 402, and GFP-PALM-L+RFP = 387. *$p < 0.05$, **$p < 0.01$. Data represent mean $\pm$ SEM. (D) Knockdown of paralemmin-1 influences the number of filopodia formed at DIV 7. Neurons were cotransfected with RFP and either with GFP or GFP-PALM-L, and scramble RNAi as a control (Ctl RNAi) or with paralemmin-1 specific RNAi (PALM RNAi). Paralemmin-1–resistant RNAi (PALM Res.) was also used to determine whether changes in filopodia number are due to specific knockdown of paralemmin-1. (E) Quantification of the number of filopodia/100 μm shows paralemmin-1 knockdown diminishes the number of filopodia formed, and these effects can be rescued upon expression PALM Res. Number of cells analyzed for each group is indicated at the bottom of each bar. Number of filopodia analyzed per group: GFP+RFP+Ctl RNAi = 666, GFP+RFP+PALM RNAi = 532, RFP+PALM-L+Ctl RNAi = 507, PALM-L+RFP+PALM RNAi = 202, and RFP+PALM-L Res+ PALM RNAi = 531. *$p < 0.05$, **$p < 0.01$, ***$p < 0.001$. Data represent mean $\pm$ SEM. Scale bars, 10 μm.

whereas the expression of the long splice variant containing exon 8 (paralemmin-L) correlates with a period of active spinogenesis (Figure 1B). Here we contrasted the effects of paralemmin-1 variants on filopodia induction in developing hippocampal neurons at DIV 7, a period that correlates with active filopodia formation. When transfected into neurons, both paralemmin-S (19.1 ± 1.2) and paralemmin-L (19.0 ± 2.1) splice variants were found to enhance the number of filopodia per 100 μm of dendritic length when compared with control cells expressing GFP (11.5 ± 1.9; Figure 1C).

We next performed knockdown experiments to investigate whether paralemmin-1 is required for filopodia induction. RNAi that specifically blocks the expression of paralemmin-1 (PALM RNAi) in both heterologous cells and neurons (GFP-actin+Ctl RNAi; 100.0 ± 8.4%); GFP-actin+PALM RNAi (46.8 ± 7.0%) was generated and characterized (Supplementary Figure 1B). Neurons were cotransfected with red fluorescent protein (RFP) and either PALM RNAi or control scramble RNAi (Ctl RNAi; Figure 1D), and changes in filopodia number were assessed by visualizing RFP-positive protrusions. Knockdown of paralemmin-1 resulted in a significant decrease in the number of filopodia per 100 μm of dendritic length (9.0 ± 1.3) when compared with neurons expressing Ctl RNAi (13.9 ± 0.8; Figure 1E). To exclude the possibility that the reduction in filopodia number upon paralemmin-1 knockdown is due to off-target effects, we generated a paralemmin-1 mutant resistant to RNAi (Figure 1D). Cotransfection of this mutant with PALM RNAi restored filopodia number to levels similar to cells transfected with wild-type paralemmin-1 and Ctl RNAi (18.5 ± 1.5; Figure 1E). Moreover, cotransfection of paralemmin-1 with PALM RNAi resulted in a similar reduction in filopodia number (6.5 ± 0.8; Figure 1E). In contrast, transfection of paralemmin-1 with Ctl RNAi resulted in a significant increase in the number of filopodia compared with GFP (Figure 1E). These results suggest that PALM RNAi is indeed specific to knockdown of paralemmin-1.

Spine Induction by Paralemmin-1 Is Regulated by Alternative Splicing and Protein Palmitoylation

Because filopodia are thought to serve as precursors for spines, the ability of paralemmin-1 to regulate filopodia induction prompted us to examine whether long-term expression of paralemmin-1 ultimately influences the number of spines (Figure 2A). This analysis was performed in neurons at DIV 12–14, a period where spines begin to emerge. Changes in the relative proportions of filopodia and spines were contrasted to Shank1b, a potent modulator of spine maturation (Sala *et al.*, 2001). Because the palmitoylation motif of paralemmin-1 fused to GFP (paralemmin CT) is sufficient to increase the number of filopodia in neuronal cells (Figure 2B), we first examined whether paralemmin-CT induced filopodia is sufficient to increase spine number. Indeed, induction of filopodia correlated with an increase in spine number in neurons transfected with paralemmin CT (Figure 2, B and C). We next contrasted the effects of paralemmin CT, paralemmin-S, and paralemmin-L expression.

Expression of both paralemmin-S (16.9 ± 1.9), paralemmin-L (26.1 ± 2.7), as well as paralemmin CT (19.3 ± 1.3), significantly increased the number of spine-like protrusions per 100 μm of dendritic length when compared with GFP-expressing cells (11.1 ± 0.7; Figure 2, B and C). The induction of filopodia and spines by paralemmin CT was comparable to paralemmin-S, indicating a significant role for the lipidated motif of paralemmin-1 in altering protrusion formation by paralemmin-S (Figure 2, B and C). In contrast, Shank1b (42.1 ± 5.8) had profound effects on spine number but did not alter the number of filopodia (Figure 2, B and C).

Next, we examined the effects of mutant forms of paralemmin-1 lacking the palmitoylated cysteines at positions 334 and 336 or a combination of the palmitoylated cysteines and the prenylated residue at position 337. Mutating any of the lipidated sites abolished the ability of paralemmin-1 to increase the number of filopodia and spines. The number of spines was reduced below control levels, suggesting a dominant-negative mechanism [paralemmin-S (C334S), 3.0 ± 0.3; paralemmin-S (C336S), 4.7 ± 0.9; paralemmin-L (C336S); paralemmin-S (C334, 336, 337S), 3.1 ± 0.4; 4.5 ± 0.8; Figure 2, B and C].

To determine whether newly formed protrusions represent sites apposed to presynaptic elements, we analyzed changes in synaptophysin-positive clusters at DIV 12–14 (Figure 2D; Supplementary Figure 2). This analysis revealed that both splice variants of paralemmin-1 increased the number, but not the size of synaptophysin-positive clusters compared with GFP (Figure 2, E and F). Expression of the palmitoylation/prenylation mutant form (paralemmin-S; C334, 336, 337S) did not alter synaptophysin cluster number, but resulted in a significant reduction in the size of synaptophysin-positive clusters compared with GFP (Figure 2, E and F), a result suggesting that expression of this mutant interferes in a dominant-negative manner with the recruitment of elements required for synapse maturation. Next, we examined whether expression of paralemmin-1 modulates postsynaptic maturation by quantifying changes in clustering of the AMPA receptor subunit, GluR1. Transfected neurons were fixed at DIV 14–16 and stained for GluR1 (Figure 3A). Both paralemmin-1 splice variants increase the number of GluR1-positive puncta; however, the effects of paralemmin-L were more dramatic (Figure 3B). Moreover, paralemmin-L, but not paralemmin-S, increased the size of GluR1 puncta in individual spines, suggesting that developmentally regulated expression of paralemmin-1 splice variants control specific steps in filopodia formation and their maturation to spines (Figure 3C).

Differential Effects of Paralemmin-1 and Shank1b on Filopodia Induction and Spine Maturation

Both paralemmin-L and Shank1b induce spine maturation; however, it is unclear whether similar mechanisms are involved. To further explore this issue, we used a heterologous expression system to determine if paralemmin-1 and Shank1b are involved in filopodia induction. We transfected COS-7 cells with either GFP, paralemmin-S, paralemmin-L, the C-terminal tail of paralemmin-1 fused to GFP (paralemmin CT), the acylation-deficient forms of paralemmin-S, the acylation-deficient form of paralemmin-L (C336S), or Shank1b, and stained with antibodies against GFP and phalloidin (Figure 4A). Both paralemmin-1 splice variants and paralemmin CT were sufficient to induce filopodia in a palmitoylation-dependent manner (Figure 4B). Conversely, Shank1b failed to induce filopodia in these cells (Figure 4B). This analysis shows that Shank1b is insufficient for filopodia induction in heterologous cells. However, it is possible that Shank1b influences filopodia induction in developing neurons. To assess this possibility, we performed a detailed time course analysis and contrasted the number of filopodia and spines formed in neurons transfected with GFP or Shank1b, 48 and 72 h after transfection (Figure 5A). Assessing protrusion type and number, we found that Shank1b expressing cells exhibited a significant increase in the number of spine-like protrusions (13 ± 1.7) 48 h after transfection when compared with GFP (3 ± 0.4) as measured per 100 μm of

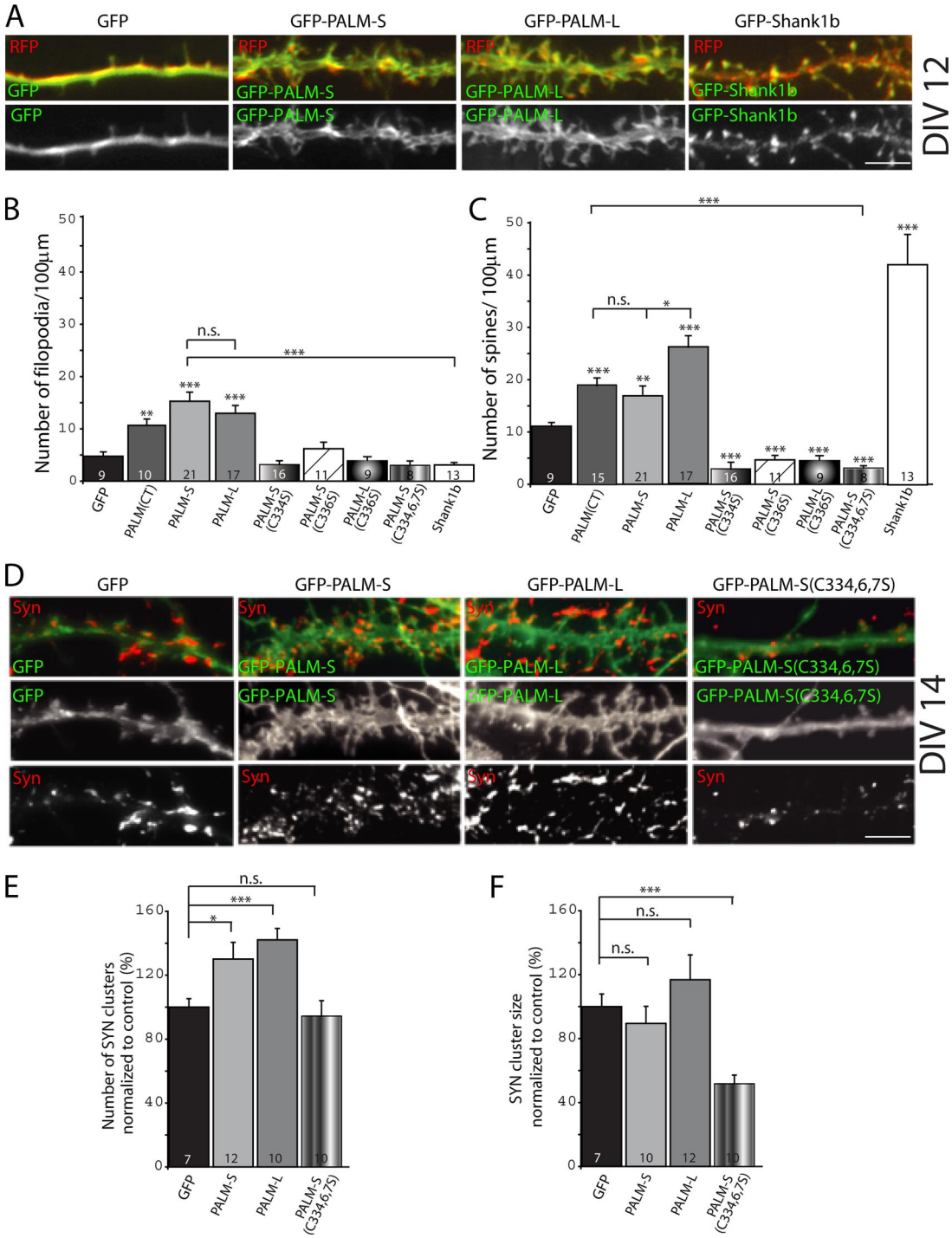

Figure 2. Long-term expression of paralemmin-1 induces spine maturation. (A and D) Effects of paralemmin-1 expression on the number of filopodia and spines formed was assessed in hippocampal neurons cotransfected with RFP (red) and either GFP (green), GFP-tagged paralemmin CT [GFP-PALM (CT)], GFP-tagged paralemmin-S (GFP-PALM-S), GFP-tagged paralemmin-L (GFP-PALM-L), mutant forms of GFP-PALM-S either lacking Cys 334 [GFP-PALM-S (C334S), Cys336 (GFP-PALM-S (C336S), or Cys334, Cys336, Cys337 (GFP-PALM-S (C334,6,7S)[, and GFP-PALM-L (C336S), at DIV 7 and fixed at DIV 12–14. Expression of various paralemmin-1 recombinant forms on dendritic protrusions was contrasted to GFP-tagged Shank1b (GFP-Shank1b). (B and C) Results show that GFP-PALM (CT), GFP-PALM-S, and GFP-PALM-L, but not the palmitoylation-deficient forms, increases the number of filopodia and spines formed. More robust effects on spine maturation were observed with GFP-PALM-L. In contrast, GFP-Shank1b overexpression enhanced spine maturation but did not alter the number of filopodia formed. (E) Dendritic protrusions induced by paralemmin-1 are synaptic. The number of synaptophysin-positive clusters were measured and normalized to controls expressing GFP. GFP-PALM-S and GFP-PALM-L but not GFP-PALM-S (C334,6,7S) significantly increased the number of synaptophysin (Syn) positive clusters when compared with GFP controls. Number of cells analyzed for each group is indicated at the bottom of each bar. Number of filopodia and spines analyzed per group in A are, respectively: GFP +RFP = 120 and 334, PALM (CT) +RFP = 628 and 878, PALM-S +RFP = 996 and 1124, PALM-L+RFP = 565 and 1386, PALM-S (C334, 6, 7S) = 86 and 76, PALM-S (C336S) = 180 and 144, PALM-S (C334S) = 187 and 118, PALM-L (C336S) = 115 and 112, and Shank1b+RFP = 103 and 1572, respectively. *$p < 0.05$, **$p < 0.01$, ***$p < 0.001$; n.s., no significant difference. Data represent mean ± SEM. Scale bars, 10 μm.

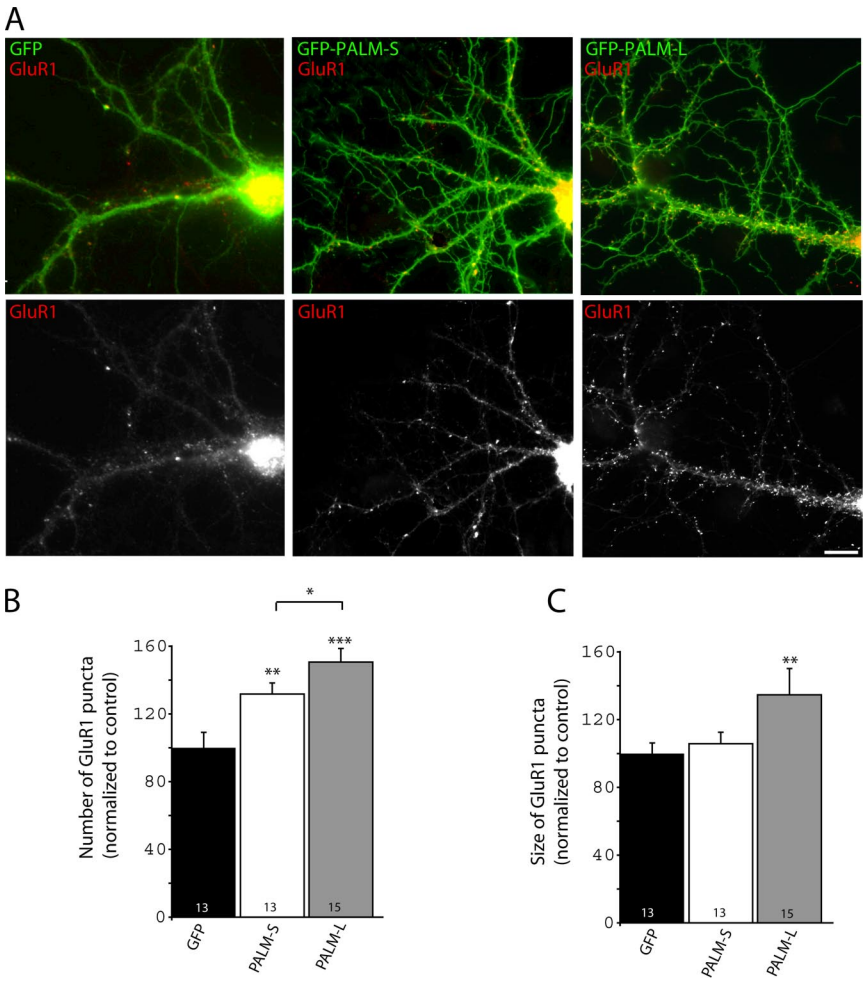

Figure 3. Differential effects of paralemmin-1 splice variants on GluR1 accumulation in dendritic spines. (A) Hippocampal neurons were transfected at DIV 7 with either GFP (green), GFP-tagged paralemmin-S (GFP-PALM-S), or GFP-tagged paralemmin-L (GFP-PALM-L) and fixed and stained with GluR1 specific antibodies (red) at DIV 14. (B) Number of GluR1 puncta was significantly increased in neurons expressing GFP-PALM-L and GFP-PALM-S when compared with GFP-expressing controls. (C) GluR1 puncta size was significantly increased in neurons expressing GFP-PALM-L but not GFP-PALM-S. Number of cells analyzed for each group is indicated at the bottom of each bar. *$p < 0.05$, **$p < 0.01$, ***$p < 0.001$. Data represent mean ± SEM. Scale bar, 10 μm.

dendritic length (Figure 5B). However, after 72-h expression, we found a small but significant reduction in the number of filopodia in Shank1b-expressing cells (5 ± 0.5) compared with GFP (11 ± 1.8). This decrease in the number of filopodia after 72-h expression correlated with a significant increase in the number of spines (24.5 ± 3.9) induced by Shank1b, suggesting that Shank1b is potentially involved in the transformation of existing filopodia to spine-like protrusions.

To further characterize the timing of filopodia transformation to spines, we performed time-lapse imaging in neurons transfected with RFP in combination with various constructs of interest at DIV 7 and imaged 2 d after transfection (Figure 5, C–E). Images were acquired every 2 min, and we focused on quantifying four major events during a 2- to 3-h imaging period: 1) spine-like protrusions that become filopodia, 2) filopodia that transform into spine-like protrusions, 3) stable filopodia, and 4) stable spine-like protrusions. This analysis revealed that within this short time scale, paralemmin-L enhanced the turnover of filopodia to spines (24 ± 3.8%) and spines to filopodia (39 ± 5.7%) compared with GFP (10 ± 1.2 and 25 ± 4.3%), respectively (Figure 5, C and F). This finding suggests that paralemmin-1 accelerates protrusion turnover and dynamics, favoring the formation of both filopodia and spine-like protrusions. Moreover, spine-like protrusions that remain stable within the entire imaging period were not significantly altered by paralemmin-L compared with GFP expressing cells, suggesting that overall; paralemmin-1 accelerates membrane dynamics and protrusion turnover in the direction of filopodia to spines, rather than destabilizing newly formed spines. In older neurons (DIV 14), however, paralemmin-L expression enhanced spine stability (66.0 ± 2.0%) when compared with GFP (50.8 ± 4.7%) controls (Supplementary Figure 5). These results may reflect a maturation stage-dependent difference in membrane dynamics in young versus old neurons.

In contrast with the moderate effects of paralemmin-1 manifested on spine stabilization in DIV 9 neurons, the number of events in which existing filopodia transform into spine-like protrusions was significantly increased in Shank1b-expressing cells (Shank1b; 36.0 ± 4.3%, paralemmin-L; 23.5 ± 3.7%, GFP; 9.8 ± 1.2%; Figure 5, E and F). Moreover, the number of stable spine-like protrusions in Shank1b-expressing cells was greater than paralemmin-L (Shank1b; 31.6 ± 4.1%, paralemmin-L; 12.4 ± 1.9%) and GFP-expressing neurons (20.6 ± 2.7%) (Figure 5, D and F). These results reveal that paralemmin-1 effects on spine maturation are slow, requiring several days, and most likely this process involves recruitment of other molecules to coordinate their transformation into spines. In contrast, transformation of filopodia into spines occurs rapidly in Shank1b-overexpressing cells, on the time scale of minutes to hours (Figure 5, E and F). These results hint to a mechanism by which recruitment of mobile transport packets of proteins to filopodia stabilizes dendritic protrusions (Marrs *et al.*, 2001; Prange and Murphy, 2001). Mobile clusters containing PSD-95 and Shank1b do exist (Gerrow *et al.*, 2006) and thus,

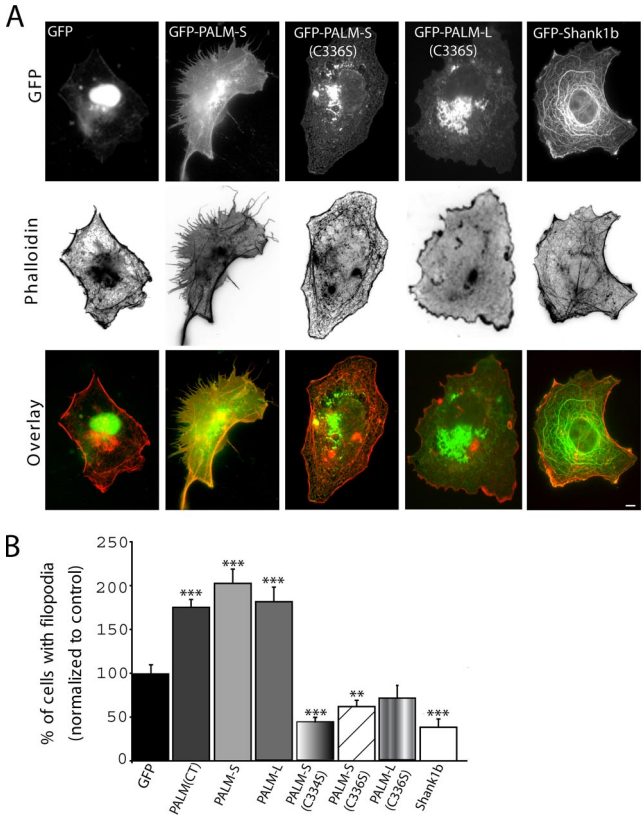

Figure 4. Induction of filopodia by paralemmin-1 but not Shank1b in COS-7 cells. (A) Various constructs fused to GFP (green) were transfected into COS-7 cells, fixed, and stained with rhodamine-conjugated phalloidin (red). Representative images of cells transfected with either GFP (green), GFP-tagged paralemmin CT (GFP-PALM(CT)), GFP-tagged paralemmin-S (GFP-PALM-S), palmitoylation mutant forms of paralemmin-1 lacking Cys 336 (GFP-PALM-S (C336S), GFP-PALM-L (C336S), or GFP-tagged Shank1b (GFP-Shank1b) are shown in top panels. (B) Quantification of filopodia induction was measured by counting the number of cells that showed filopodia outgrowth. Cells immunolabeled for phalloidin are shown in middle panels. Analysis demonstrates that wild-type forms of paralemmin-1 but not the palmitoylation deficient forms or Shank1b significantly increase the number of cells with filopodia when compared with GFP-expressing cells. Additionally, appending the C-terminal acylated motif of paralemmin-1 to GFP [GFP-PALM(CT)] is sufficient for filopodia induction in COS-7 cells. Number of cells analyzed for each group, ≥69. $^{**}p < 0.01$, $^{***}p < 0.001$. Data represent mean ± SEM. Scale bar, 5 μm.

one possibility is that recruitment of a scaffold protein complex containing Shank1b to filopodia plays a role in the stabilization of these structures.

The enhanced transformation of filopodia to spines by Shank1b suggests that its expression would potentiate paralemmin-1 effects on spine induction. To explore this possibility, the effects of coexpression of GFP-paralemmin-L and HA-Shank1b on spine number was examined. For this analysis, neurons were transfected at DIV 7 and fixed and stained at DIV 12, using GFP and HA antibodies, respectively. Indeed, neurons cotransfected with Shank1b and PALM-L (42.5 ± 2.6) showed a significant increase in the number of spines per 100 μm of dendritic length when compared with either GFP+RFP- (15.5 ± 2.8) or paralemmin-L+RFP– (26.8 ± 3.6) expressing cells (Supplementary Figure 4B). These results are consistent with a facilitative role for Shank1b in stabilization and maturation of protrusions induced by paralemmin-L.

We next evaluated the effects of long-term knockdown of paralemmin-1 on spine development in mature neurons (DIV 12–14). Knockdown of paralemmin-1 results in a significant reduction in the number of spines compared with control RNAi (PALM RNAi, 53 ± 6%; Ctl RNAi, 100 ± 13%; Figure 6, A and B). Moreover, paralemmin-1 knockdown compromised Shank1b effects on spine maturation (Figure 6, C and D). These results suggest the involvement of paralemmin-1 in Shank1b induced effects on spine maturation (Figure 6D). It is important to note that aberrant dendritic growth and the formation of short neurites was also observed in ~30% of neurons after prolonged (7–10 d) knockdown of paralemmin-1 (data not shown). These results indicate that paralemmin-1 may generally participate in events that regulate membrane dynamics, protrusion formation, and dendritic arborization.

Neuronal Activity Enhances Membrane Localization of Paralemmin-1

Neuronal activity modulates protrusion formation, which in turn fine tunes synaptic strength and plasticity (Dunaevsky *et al.*, 1999; Fischer *et al.*, 2000; Nimchinsky *et al.*, 2002; Richards *et al.*, 2005; Zuo *et al.*, 2005a,b). This process is thought to be mediated by the recruitment of proteins that alter membrane and cytoskeletal dynamics. Thus, we addressed whether neuronal activity regulates paralemmin-1 localization and function. To explore whether depolarization of hippocampal neurons has an effect on paralemmin-1 localization, DIV 16–18 hippocampal neurons were stimulated with 90 mM KCl for 3 min, after which neurons were fixed and stained for endogenous paralemmin-1. This analysis revealed a significant increase in paralemmin-1 localization at the plasma membrane (Figure 7A). To further confirm translocation of paralemmin-1 to cellular membranes, we performed subcellular fractionation and assessed the amounts of paralemmin-1 in the soluble and membrane fractions after 3 min treatment with 90 mM KCl. Indeed, this treatment resulted in an increase in the amounts of paralemmin-1 detected in the membrane fraction, as determined by calculating the amount of paralemmin-1 in the soluble/pellet (membrane) fractions and expressing it as a percent. Paralemmin-1 levels in the pellet fractions of treated cells (58.1 ± 7.7%, $^{*}p < 0.02$) were higher than those of untreated controls (45.0 ± 5.8%, $^{*}p < 0.02$). However, we found no significant change in the amounts of transferrin (pellet/load) between controls (105.3 ± 11.6%) and treated groups (113.6 ± 6.9%). This parallels the enhanced paralemmin-1 localization at the membrane as seen in Figure 7, A and B.

To address the possibility that depolarization by KCl may have resulted in nonspecific effects on membrane integrity and dynamics, we used a second approach to manipulate neuronal activity and examine changes in membrane localization of paralemmin-1. For this analysis, neurons were grown on silicon wafers and imaged using a photoconductive stimulation paradigm to induce neuronal excitability (Colicos *et al.*, 2001; Figure 7C). Analysis of the average pixel value of surface versus intracellular paralemmin-L signal shows an increase in its membrane localization, similar to the level observed with KCl treatment (Figure 7D). This confirms that paralemmin-1 localization can be modulated by physiological neuronal activity.

Next, we explored whether general manipulation of palmitoylation serves as a signal that controls activity-mediated paralemmin-1 localization at the plasma membrane. For this analysis, we treated neurons with 20 μM

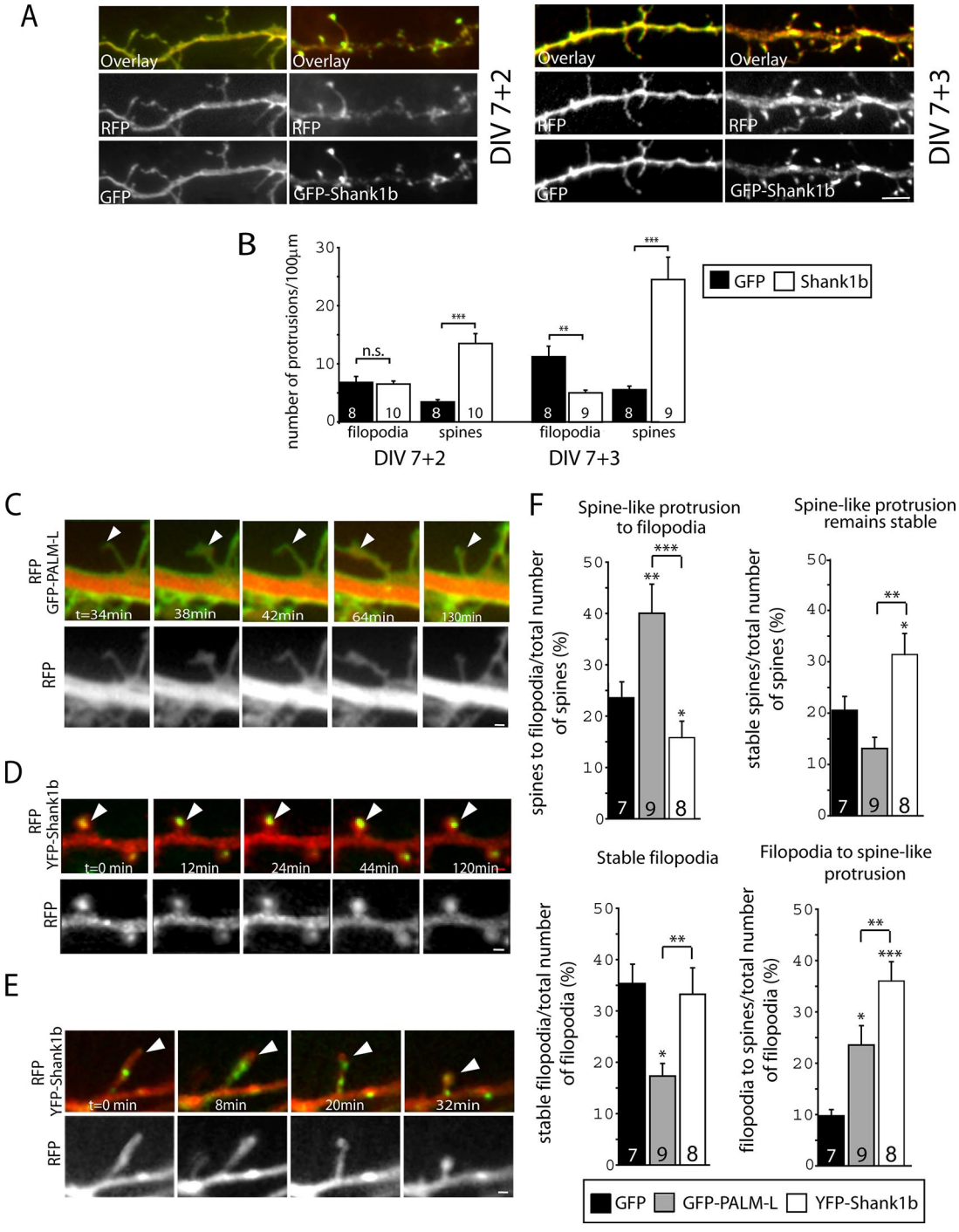

Figure 5. Shank1b but not paralemmin-1 induces rapid protrusion transformation from filopodia to spine-like structures. (A) Neurons were transfected with RFP- and GFP-tagged Shank1b (GFP-Shank1b) at DIV 7 and then fixed at either DIV 9 or 10. GFP-Shank1b expression decreases the ratio of filopodia to spines formed when compared with neurons expressing GFP. (B) Quantification of changes in dendritic protrusions per unit length. (C–E) Hippocampal neurons were transfected with RFP and either with GFP, GFP-tagged paralemmin-L (GFP-PALM-L) or YFP-tagged Shank1b (YFP-Shank1b) at DIV 7 and then imaged at DIV 9 using time-lapse microscopy. Images were acquired every 2 min. In C, these images represent a transition from a filopodium (t = 34 and 42 min) to a spine-like protrusion at (t = 38 and 130 min). In D, these images represent a spine induced by Shank1b that remained stable from t = 0 min to t = 120 min. In E, at t = 0 min, the image shows a filopodia-like protrusion containing a Shank1b cluster that retracts to form a spine-like protrusion at t = 32 min and remains stable. (F) Analysis revealed differential effects of GFP-PALM-L on protrusion dynamics. Most significant is enhanced membrane dynamics and protrusion turnover in cells expressing GFP-PALM-L as well as the number of stable spines in neurons expressing YFP-Shank1b but not GFP-PALM-L on a time scale of 2–3 h. Number of cells analyzed for each group is indicated at the bottom of each bar. Number of filopodia and spines analyzed per group in A are as follows: DIV 7 + 2: GFP+RFP = 127 and 62 and GFP-Shank1b+RFP = 178 and 375; DIV 7 + 3: GFP+RFP = 240 and 123 and GFP-Shank1b+RFP = 135 and 641. White arrowheads denote dendritic protrusions. *$p < 0.05$, **$p < 0.01$, ***$p < 0.001$; n.s. = no significant difference. Data represent mean ± SEM. Scale bar, (A) 10 μm; (C–E) 1 μm.

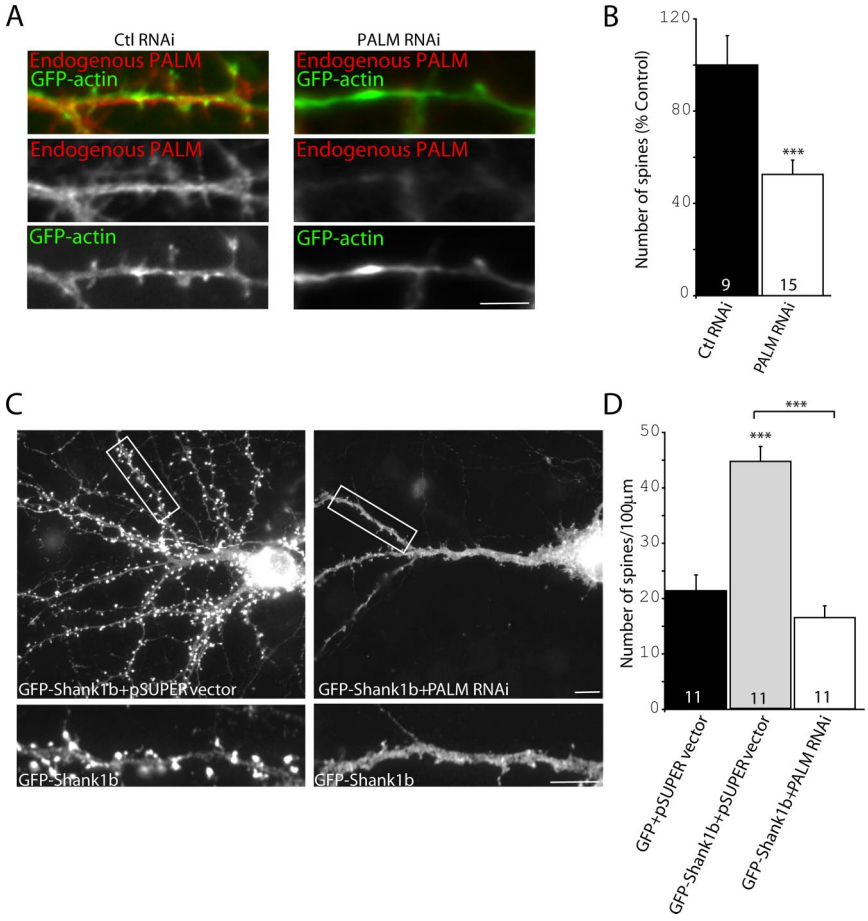

Figure 6. Effects of long-term knockdown of paralemmin-1 on spine formation. (A) Hippocampal neurons were cotransfected with GFP-actin and either with control RNAi (Ctl RNAi) or paralemmin-1–specific RNAi (PALM RNAi) at DIV 5. Neurons were then fixed and stained for endogenous paralemmin-1 (Endogenous PALM) at DIV 12–14. (B) Quantification of dendritic spines normalized to Ctl RNAi group. There is a significant reduction in dendritic spines in neurons transfected with PALM RNAi. (C) Hippocampal neurons cotransfected with GFP or GFP-Shank1b and either with empty pSUPER vector or with PALM RNAi. (D) Quantification of GFP-Shank1b–positive spines upon knockdown of paralemmin-1. A significant reduction in GFP-Shank1b clustering as well as the number of Shank1b-positive dendritic spines in neurons transfected with GFP-Shank1b and PALM RNAi compared with controls expressing GFP-Shank1b and empty pSUPER vector. Number of cells analyzed for each group is indicated at the bottom of each bar. Number of filopodia and spines analyzed per group in B are as follows: GFP-actin+Ctl RNAi = 316 and 281, GFP-actin+PALM RNAi = 230 and 176. Number of spines analyzed per group in D is as follows: GFP+pSUPER vector = 1039, GFP Shank1b+pSUPER vector = 1564, and GFP Shank1b+PALM RNAi = 446. ***$p < 0.001$. Data represent mean ± SEM. Scale bar, (A) 5 μm; (C) 10 and 5 μm (magnified dendrite).

2-BP, a competitive inhibitor of palmitoylation, 4 h before stimulation with KCl (Webb *et al.*, 2000; El-Husseini Ael and Bredt, 2002; Gauthier-Campbell *et al.*, 2004). This treatment reduced paralemmin-1 expression at the membrane in basal conditions (Figure 7A, lower inset, and B). 2-BP also compromised paralemmin-1 localization to the membrane upon depolarization (Figure 7A, lower inset, and B). Taken together, these results suggest that blocking palmitoylation interferes with the localization of paralemmin-1 to the membrane upon enhanced synaptic activity.

Paralemmin-1 Potentiates Activity-driven Membrane Expansion

Changes in neuronal activity have been proposed to influence protrusion size and dynamics (Dunaevsky *et al.*, 1999; Fischer *et al.*, 2000; Nimchinsky *et al.*, 2002; Richards *et al.*, 2005; Zuo *et al.*, 2005a,b). The rapid translocation of paralemmin-1 to the plasma membrane upon stimulation of neuronal activity prompted us to examine whether paralemmin-1 modulates activity-driven changes in dendritic protrusions. Time-lapse imaging of DIV 9 neurons was used to assess changes in the size of protrusions within 10 min of treatment with 50 mM KCl (Figure 8A). Four common effects of paralemmin-1 on membrane expansion were measured: membrane expansion at the tip of filopodia (Figure 8A, example 1), formation of growth cone-like protrusions (Figure 8A, example 2), enlargement of existing protrusions (Figure 8A, example 3), and formation of lamellopodia-like structures at the base of protrusions (Figure 8A, example 4; Supplementary Figure 3B). Paralemmin-1 significantly enhanced membrane expansion of these irregularly shaped protrusions after KCl stimulation (Supplementary Figure 3). Analysis of GFP+Ctl RNAi (17.9 ± 1.9%) transfected controls shows that stimulation with KCl results in a small but significant increase in protrusion size, and this effect is significantly reduced in neurons coexpressing GFP+PALM RNAi (11.2 ± 1.3%; Figure 8, B and C). Expression of wild-type paralemmin-1, but not the palmitoylation-deficient forms GFP-PALM-S (C336S), GFP-PALM-S (C334,6,7S) further enhanced activity-driven protrusion expansion (Figure 8C, Figure S3). Taken together, these results reveal that paralemmin-1 recruitment to the plasma membrane is modulated by palmitoylation and that activity-driven changes in paralemmin-1 localization serve to modulate membrane expansion at the tip and base of dendritic protrusions.

DISCUSSION

In the present work, we reveal that manipulations of paralemmin-1 expression modulate filopodia induction and synapse formation. Long-term expression of paralemmin-1 induces spine maturation, as shown by its influence on the number of mature spines formed and recruitment of AMPA receptors. Moreover, this process is regulated by alternative splicing of exon 8. We demonstrate that paralemmin-1 modulates protrusion dynamics and expansion and that these effects are rapidly accelerated upon neuronal depolarization. Enhanced neuronal activity also leads to rapid redistribution of paralemmin-1 to the plasma membrane, suggesting a

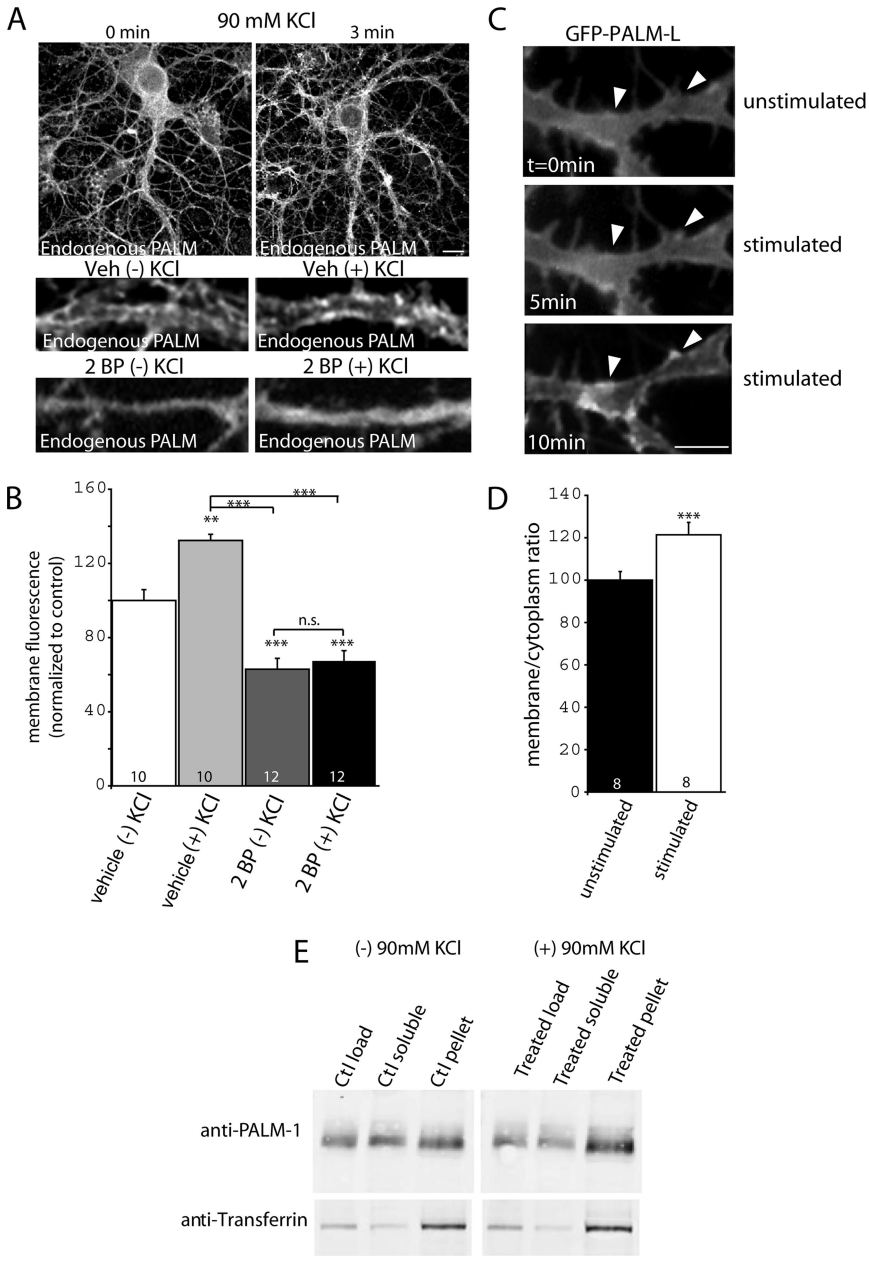

Figure 7. Neuronal activity modulates paralemmin-1 localization. (A) Hippocampal neurons were treated with 90 mM KCl or vehicle control for 3 min and fixed and stained for endogenous paralemmin-1 (Endogenous PALM). Endogenous PALM accumulation at the plasma membrane is enhanced after stimulation with 90 mM KCl when compared with untreated cells. 2-bromopalmitate (2-BP) treatment reduces Endogenous PALM accumulation at the plasma membrane at basal conditions and after KCl treatment. (B) Graph showing quantification of changes in Endogenous PALM accumulation at the membrane across four treatment groups. (C) Photoconductive stimulation increases GFP-paralemmin-L accumulation at the plasma membrane. Neurons were transfected with GFP-tagged paralemmin-L (GFP-PALM-L) and then imaged for several minutes before stimulation. White arrowheads indicate changes in accumulation of paralemmin-L before and after electrical stimulation. (D) Quantification showing a significant increase in GFP-PALM-L accumulation at the plasma membrane compared with unstimulated neurons. (E) Changes in paralemmin-1 levels in the membrane fraction after KCl treatment. Cortical neurons at DIV 16–20 were treated for 3 min with 90 mM KCl and changes in paralemmin-1 distribution was examined by subcellular fractionation. Quantification of paralemmin-1 levels in the membrane fraction was determined by calculating the amount of paralemmin-1 in the soluble/pellet fractions. Paralemmin-1 levels in the pellet (membrane) fractions of treated cells (58.1 ± 7.7%; *$p < 0.02$) were higher than those of untreated controls (45.0 ± 5.8%; *$p < 0.02$). There were no significant changes in the amounts of transferrin in the membrane fractions across groups; $p = 0.75$. Number of cells analyzed for each group is indicated at the bottom of each bar. **$p < 0.01$, ***$p < 0.001$; n.s. = no significant difference. Data represent mean ± SEM. Scale bar, (A) 10 μm; (C) 5 μm.

paralemmin-based mechanism for the effects of neuronal activity on dendritic protrusion dynamics.

Although these activity-dependent changes indicate an important role for palmitoylation in regulating paralemmin-1–induced changes in protrusion dynamics, it is important to note that treatment with 2-BP may have also indirectly affected palmitoylation and/or function of other proteins involved in this process. Future studies are needed to directly assess the effects of neuronal activity on palmitate turnover on paralemmin-1 to solidify these conclusions.

Filopodia are thought to play an active role in the initiation of synaptic contacts (Dailey and Smith, 1996; Ziv and Smith, 1996; Marrs *et al.*, 2001; Calabrese *et al.*, 2006). Furthermore, the appearance of filopodia before the formation of spines and the fact that some filopodia retract into a more stable spine-like shape has led to the hypothesis that some spines originate directly from filopodia (Fiala *et al.*, 1998; Zuo *et al.*, 2005a). In this study, we found that the majority of protrusions induced by paralemmin-1 are positive for synaptophysin and AMPA receptors. These results suggest that paralemmin-1 expression enhances the formation of synapses. Moreover, the enhanced filopodia formation correlates with an increase in spine number, supporting a role for filopodia in spine development. Consistent with these findings, knockdown of paralemmin-1 reduces filopodia formation in young neurons, as well as the development of spines in mature neurons. Thus, our results suggest that contacts between dendritic filopodia and presynaptic cells act as precursors for future spines, and ultimately, functional synapses.

We have previously shown that the palmitoylation motif fused to paralemmin-1 (paralemmin CT) is sufficient to increase the number of dendritic branches in neurons (Gauthier-Campbell *et al.*, 2004). Here we show that induction of filopodia and spines by paralemmin CT was comparable to paralemmin-S, suggesting a significant role

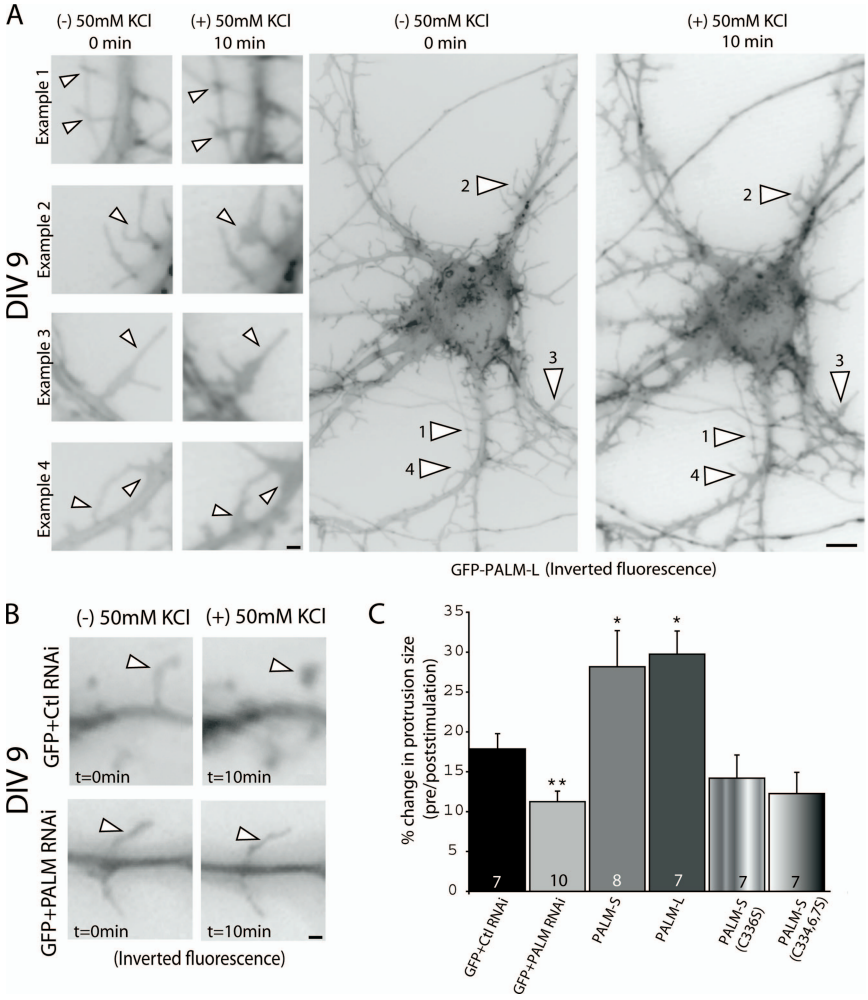

Figure 8. Activity-induced changes in dendritic protrusions are modulated by paralemmin-1. (A) Paralemmin-1 modulates neuronal activity-driven changes in protrusion size. Hippocampal neurons were transfected at DIV 7 with GFP+Ctl RNAi, GFP+PALM RNAi, GFP-tagged paralemmin-1 splice variants GFP-PALM-L, GFP-PALM-S, or the cysteine mutant forms GFP-PALM-S (C336S) or GFP-PALM-S (C334S, C336S, C337S) and then imaged at DIV 9. Images were captured before and after 10 min treatment with 50 mM KCl. Images of inverted fluorescence are shown to better visualize protrusions. Four examples of dendritic protrusion expansion are shown before and after stimulation with 50 mM KCl. Example 1, filopodia expanded at the tips; example 2, formation of a growth cone-like protrusion; example 3, enlargement of an existing protrusion; and example 4, formation of lamellopodia-like structures at the base of the protrusion. Images shown here represent inverted fluorescence for greater clarity. (B) Example of protrusion expansion in GFP+Ctl RNAi at DIV 9 after stimulation with 50 mM KCl for 10 min, and this effect is reduced in cells coexpressing GFP+PALM RNAi. Images shown here represent inverted fluorescence for greater clarity. (C) Treatment with KCl results in a small but significant increase in protrusion size in GFP+Ctl RNAi-transfected controls. Coexpression of GFP+ PALM RNAi significantly reduces the effect on protrusion expansion. Expression of GFP-PALM-S and GFP-PALM-L but not the acylation mutant forms of PALM-S significantly enhanced dendritic protrusion expansion. Protrusion diameter was measured at the base and tips, before and after stimulation and expressed as a percent change. Arrowheads point to expanded protrusions. Number of cells analyzed for each group is indicated at the bottom of each bar. *$p < 0.05$, **$p < 0.01$. Data represent mean ± SEM. Scale bar, (A, right panels) 5 μm; (A, left insets), 2 μm; and (B) 2 μm.

for the lipidated motif of paralemmin-1 in altering protrusion formation by paralemmin-S. These results also indicate that enhanced filopodia number per se contributes to the increase in spine density. However, paralemmin-L has a stronger effect on spine formation than paralemmin-S, revealing that protein–protein interactions regulated by alternative splicing modulate the efficacy of paralemmin-1 effects on spine maturation. Future experiments focused on identification of molecules that specifically associate with the paralemmin-1 isoform containing exon 8 may help clarify the differential effects induced by paralemmin-1 splice variants on spine maturation and AMPA receptor recruitment. Interestingly, the variant lacking exon 8 (paralemmin-S) is expressed at high levels at early stages of postnatal development, whereas the expression of the variant containing exon 8 (paralemmin-L) peaks at P14 (Kutzleb *et al.*, 1998). Thus, sequential expression of paralemmin-1 splice variants may contribute to filopodia induction and their subsequent transformation to spines.

The differential effects of paralemmin-1 and Shank1b on filopodia induction and spine maturation on both short- and long-term time scales are noteworthy. Expression of paralemmin-1 induces filopodia in both heterologous cells and neurons. In contrast, Shank1b fails to induce filopodia in both cell types. Interestingly, these changes correlate with a rapid increase in the number of spine-like structures. Consistent with these findings, live imaging over a period of hours revealed that Shank1b expression increases the number of events where filopodia transform into spine-like structures, suggesting that Shank1b functions to rapidly induce the transformation of existing filopodia into spines. Within this short time scale, paralemmin-L enhanced the turnover of filopodia to spines and vice versa. Moreover, spine-like protrusions that remain stable within the entire imaging period were not significantly enhanced by paralemmin-1 compared with GFP, suggesting that overall, paralemmin-L accelerates membrane dynamics and protrusion turnover in the direction of filopodia to spines, rather than destabilizing newly formed spines. Overall, these results reveal more robust effects of Shank1b on filopodia transformation to spines. These data suggest that paralemmin-L induced effects on spine maturation require several days and that this process most likely requires recruitment of additional molecules for spine stabilization.

The effect of coexpression of paralemmin-L with Shank1b led to a significant increase in spine number when compared with expression of paralemmin-L alone. These results are consistent with a facilitative role for Shank1b in stabilization and maturation of protrusions induced by paralemmin-L. However, it is important to note that the combined effects of these proteins were not significantly larger than those observed in neurons expressing Shank1b alone, suggesting

that the conversion of filopodia to spines is a bottleneck point, being limited by Shank1b and/or its supporting molecular machinery with respect to this process. Moreover, the ability of Shank1b to transform filopodia into spines becomes saturated, in that its effects are maximized with time. These results are in contrast with the knockdown findings, which show that loss of paralemmin-1 reduces Shank1b-induced effects on spine maturation, indicating that loss of filopodia compromises the effects of Shank1b on spine induction.

The actin cytoskeleton plays a fundamental role in regulating process outgrowth through changes in membrane dynamics. Despite the changes in membrane dynamics observed in this study, it remains unclear how paralemmin-1 induces its effects on protrusion extension. Previous work indicates that alterations of membrane geometry induce changes in membrane curvature and the extension of membrane protrusions (Raucher and Sheetz, 2000; Marguet *et al.*, 2006). This process can be regulated by activation of phospholipase C and plasma membrane phosphatidylinositol 4,5-bisphosphate, which act to regulate adhesion between the cytoskeleton and the plasma membrane.

The functions of several acylated proteins implicated in filopodia induction, including GAP-43 (Strittmatter *et al.*, 1994) and Wrch, a Wnt-regulated Cdc42 homolog (Berzat *et al.*, 2005), seem to rely on protein palmitoylation. Thus, palmitoylation seems to exert specific effects that regulate induction of protrusion formation. It is tempting to speculate that the insertion of palmitoyl groups into membranes, which relies on the motif structure and spacing between the acylated cysteines, directly triggers membrane deformity and alters membrane flow, which in turn results in modulation of protrusion extension. Alternatively, altered membrane dynamics may indirectly regulate recruitment of actin-bundling proteins and GTPases that regulate protrusion formation. It is also possible that palmitoylation-dependent targeting of paralemmin-1 and other palmitoylated proteins to lipid rafts affects signaling molecules that reside in these lipid microdomains, resulting in the activation of molecules directly involved in protrusion expansion (Anderson and Jacobson, 2002; Gauthier-Campbell *et al.*, 2004; Kutzleb *et al.*, 2007). Alterations in cholesterol/sphingolipid-enriched lipid raft microdomains in neurons influence protein trafficking, formation of signaling complexes, and regulation of the actin cytoskeleton (Hering *et al.*, 2003). For example, depletion of cholesterol/sphingolipids leads to gradual loss of synapses and dendritic spines, as well as instability of surface AMPA receptors, which, along with other postsynaptic proteins, have been shown to be associated with lipid rafts in dendrites (Hering *et al.*, 2003). Others have shown that cholesterol promotes synapse maturation in retinal ganglion cells, suggesting that alterations in lipid raft integrity and/or constituents directly influence synapse density and morphology (Mauch *et al.*, 2001; Goritz *et al.*, 2005). These findings offer a potential link between disordered lipid composition and the loss of synapses seen in brain disorders such as Down syndrome, where loss of dendritic spines and altered phospholipid composition has been documented (Murphy *et al.*, 2000). It will be important, next, to examine whether enhanced incorporation of palmitoylated paralemmin-1 into lipid rafts triggers recruitment of molecules that control cytoskeleton dynamics and membrane expansion to induce protrusion formation.

Activity-dependent alterations in spine dynamics, spine enlargement, and recruitment of AMPA receptors have been associated with changes incurred during learning paradigms, and in particular, changes in synaptic and structural plasticity, including induction of LTP (Bredt and Nicoll, 2003). Paralemmin-1 expression persists in the adult brain, and thus paralemmin-1 may also be involved in regulation of spine morphology and protrusion expansion in response to synaptic activity or plasticity. The activity-driven changes we observed in protrusion expansion upon expression of paralemmin-1 in developing neurons lend further support to this notion. Next, it will be important to determine whether specific paradigms that influence postsynaptic receptor stimulation and neurotransmitter release exert specific effects on paralemmin-1 localization and protrusion expansion in older neurons. Application of pharmacological reagents that manipulate synaptic function will clarify further activity-induced changes in paralemmin-1 localization and action. Studies focused on analyzing the effects of paralemmin-1 on protrusion formation and expansion in mature neurons in response to specific plasticity-associated learning paradigms will help address this possibility.

ACKNOWLEDGMENTS

Alaa El-Husseini passed away in a tragic accident on December 23, 2007. As a great friend and mentor, he will be deeply missed. We thank Esther Yu and Xiao-Yan Jiang for the preparation of cells and general lab reagents. We thank Kimberly Gerrow, Dr. Changiz Taghibiglou, and Alan Baggish for their excellent advice throughout this project. This work was supported by grants to A.E.H. from the Canadian Institutes for Health Research (CIHR), the Michael Smith foundation for Health Research, the EJLB Foundation, and Neuroscience Canada. A.E.H. is an MSFHR senior scholar. T.H.M. was supported in part by an operating grant from CIHR (MOP-12675). This work was further supported by grants from Deutsche Forschungsgemeinschaft and Vetenskapsradet to M.W.K. Finally, M.A.C. was supported by Alberta Ingenuity Fund and AHFMR.

REFERENCES

Anderson, R. G., and Jacobson, K. (2002). A role for lipid shells in targeting proteins to caveolae, rafts, and other lipid domains. Science *296*, 1821–1825.

Basile, M., Lin, R., Kabbani, N., Karpa, K., Kilimann, M., Simpson, I., and Kester, M. (2006). Paralemmin interacts with D3 dopamine receptors: implications for membrane localization and cAMP signaling. Arch. Biochem. Biophys. *446*, 60–68.

Berzat, A. C., Buss, J. E., Chenette, E. J., Weinbaum, C. A., Shutes, A., Der, C. J., Minden, A., and Cox, A. D. (2005). Transforming activity of the Rho family GTPase, Wrch-1, a Wnt-regulated Cdc42 homolog, is dependent on a novel carboxyl-terminal palmitoylation motif. J. Biol. Chem. *280*, 33055–33065.

Bredt, D. S., and Nicoll, R. A. (2003). AMPA receptor trafficking at excitatory synapses. Neuron *40*, 361–379.

Burwinkel, B., Miglierini, G., Jenne, D. E., Gilbert, D. J., Copeland, N. G., Jenkins, N. A., Ring, H. Z., Francke, U., and Kilimann, M. W. (1998). Structure of the human paralemmin gene (PALM), mapping to human chromosome 19p13.3 and mouse chromosome 10, and exclusion of coding mutations in grizzled, mocha, jittery, and hesitant mice. Genomics *49*, 462–466.

Calabrese, B., Wilson, M. S., and Halpain, S. (2006). Development and regulation of dendritic spine synapses. Physiology (Bethesda) *21*, 38–47.

Castellini, M., Wolf, L. V., Chauhan, B. K., Galileo, D. S., Kilimann, M. W., Cvekl, A., and Duncan, M. K. (2005). Palm is expressed in both developing and adult mouse lens and retina. BMC Ophthalmol. *5*, 14–24.

Colicos, M. A., Collins, B. E., Sailor, M. J., and Goda, Y. (2001). Remodeling of synaptic actin induced by photoconductive stimulation. Cell *107*, 605–616.

Colicos, M. A., and Syed, N. I. (2006). Neuronal networks and synaptic plasticity: understanding complex system dynamics by interfacing neurons with silicon technologies. J. Exp. Biol. *209*, 2312–2319.

Dailey, M. E., and Smith, S. J. (1996). The dynamics of dendritic structure in developing hippocampal slices. J. Neurosci. *16*, 2983–2994.

Dunaevsky, A., Tashiro, A., Majewska, A., Mason, C., and Yuste, R. (1999). Developmental regulation of spine motility in the mammalian central nervous system. Proc. Natl. Acad. Sci. USA *96*, 13438–13443.

El-Husseini Ael, D., and Bredt, D. S. (2002). Protein palmitoylation: a regulator of neuronal development and function. Nat. Rev. Neurosci. *3*, 791–802.

Fiala, J. C., Feinberg, M., Popov, V., and Harris, K. M. (1998). Synaptogenesis via dendritic filopodia in developing hippocampal area CA1. J. Neurosci. *18*, 8900–8911.

Fiala, J. C., Spacek, J., and Harris, K. M. (2002). Dendritic spine pathology: cause or consequence of neurological disorders? Brain Res. Brain Res. Rev. *39*, 29–54.

Fischer, M., Kaech, S., Knutti, D., and Matus, A. (1998). Rapid actin-based plasticity in dendritic spines. Neuron *20*, 847–854.

Fischer, M., Kaech, S., Wagner, U., Brinkhaus, H., and Matus, A. (2000). Glutamate receptors regulate actin-based plasticity in dendritic spines. Nat. Neurosci. *3*, 887–894.

Gauthier-Campbell, C., Bredt, D. S., Murphy, T. H., and El-Husseini Ael, D. (2004). Regulation of dendritic branching and filopodia formation in hippocampal neurons by specific acylated protein motifs. Mol. Biol. Cell *15*, 2205–2217.

Gerrow, K., and El-Husseini, A. (2006). Cell adhesion molecules at the synapse. Front. Biosci. *11*, 2400–2419.

Gerrow, K., Romorini, S., Nabi, S. M., Colicos, M. A., Sala, C., and El-Husseini, A. (2006). A preformed complex of postsynaptic proteins is involved in excitatory synapse development. Neuron *49*, 547–562.

Goda, Y., and Colicos, M. A. (2006). Photoconductive stimulation of neurons cultured on silicon wafers. Nat. Protoc. *1*, 461–467.

Goritz, C., Mauch, D. H., and Pfrieger, F. W. (2005). Multiple mechanisms mediate cholesterol-induced synaptogenesis in a CNS neuron. Mol. Cell Neurosci. *29*, 190–201.

Hall, A., and Nobes, C. D. (2000). Rho GTPases: molecular switches that control the organization and dynamics of the actin cytoskeleton. Philos. Trans. R. Soc. Lond. B. Biol. Sci. *355*, 965–970.

Halpain, S., Spencer, K., and Graber, S. (2005). Dynamics and pathology of dendritic spines. Prog. Brain Res. *147*, 29–37.

Hering, H., Lin, C. C., and Sheng, M. (2003). Lipid rafts in the maintenance of synapses, dendritic spines, and surface AMPA receptor stability. J. Neurosci. *23*, 3262–3271.

Hering, H., and Sheng, M. (2001). Dendritic spines: structure, dynamics and regulation. Nat. Rev. Neurosci. *2*, 880–888.

Huang, K. *et al.* (2004). Huntingtin-interacting protein HIP14 is a palmitoyl transferase involved in palmitoylation and trafficking of multiple neuronal proteins. Neuron *44*, 977–986.

Kang, R., Swayze, R., Lise, M. F., Gerrow, K., Mullard, A., Honer, W. G., and El-Husseini, A. (2004). Presynaptic trafficking of synaptotagmin I is regulated by protein palmitoylation. J. Biol. Chem. *279*, 50524–50536.

Kirov, S. A., Petrak, L. J., Fiala, J. C., and Harris, K. M. (2004). Dendritic spines disappear with chilling but proliferate excessively upon rewarming of mature hippocampus. Neuroscience *127*, 69–80.

Kutzleb, C., Petrasch-Parwez, E., and Kilimann, M. W. (2007). Cellular and subcellular localization of paralemmin-1, a protein involved in cell shape control, in the rat brain, adrenal gland and kidney. Histochem. Cell Biol. *127*, 13–30.

Kutzleb, C., Sanders, G., Yamamoto, R., Wang, X., Lichte, B., Petrasch-Parwez, E., and Kilimann, M. W. (1998). Paralemmin, a prenyl-palmitoyl-anchored phosphoprotein abundant in neurons and implicated in plasma membrane dynamics and cell process formation. J. Cell Biol. *143*, 795–813.

Lim, S., Naisbitt, S., Yoon, J., Hwang, J. I., Suh, P. G., Sheng, M., and Kim, E. (1999). Characterization of the Shank family of synaptic proteins. Multiple genes, alternative splicing, and differential expression in brain and development. J. Biol. Chem. *274*, 29510–29518.

Marguet, D., Lenne, P. F., Rigneault, H., and He, H. T. (2006). Dynamics in the plasma membrane: how to combine fluidity and order. EMBO J. *25*, 3446–3457.

Marrs, G. S., Green, S. H., and Dailey, M. E. (2001). Rapid formation and remodeling of postsynaptic densities in developing dendrites. Nat. Neurosci. *4*, 1006–1013.

Matus, A. (2005). Growth of dendritic spines: a continuing story. Curr. Opin. Neurobiol. *15*, 67–72.

Mauch, D. H., Nagler, K., Schumacher, S., Goritz, C., Muller, E. C., Otto, A., and Pfrieger, F. W. (2001). CNS synaptogenesis promoted by glia-derived cholesterol. Science *294*, 1354–1357.

Murphy, E. J., Schapiro, M. B., Rapoport, S. I., and Shetty, H. U. (2000). Phospholipid composition and levels are altered in Down syndrome brain. Brain Res. *867*, 9–18.

Nimchinsky, E. A., Sabatini, B. L., and Svoboda, K. (2002). Structure and function of dendritic spines. Annu. Rev. Physiol. *64*, 313–353.

Portera-Cailliau, C., Pan, D. T., and Yuste, R. (2003). Activity-regulated dynamic behavior of early dendritic protrusions: evidence for different types of dendritic filopodia. J. Neurosci. *23*, 7129–7142.

Prange, O., and Murphy, T. H. (2001). Modular transport of postsynaptic density-95 clusters and association with stable spine precursors during early development of cortical neurons. J. Neurosci. *21*, 9325–9333.

Raucher, D., and Sheetz, M. P. (2000). Cell spreading and lamellipodial extension rate is regulated by membrane tension. J. Cell Biol. *148*, 127–136.

Richards, D. A., Mateos, J. M., Hugel, S., de Paola, V., Caroni, P., Gahwiler, B. H., and McKinney, R. A. (2005). Glutamate induces the rapid formation of spine head protrusions in hippocampal slice cultures. Proc. Natl. Acad. Sci. USA *102*, 6166–6171.

Sala, C., Piech, V., Wilson, N. R., Passafaro, M., Liu, G., and Sheng, M. (2001). Regulation of dendritic spine morphology and synaptic function by Shank and Homer. Neuron *31*, 115–130.

Strittmatter, S. M., Igarashi, M., and Fishman, M. C. (1994). GAP-43 amino terminal peptides modulate growth cone morphology and neurite outgrowth. J. Neurosci. *14*, 5503–5513.

Webb, Y., Hermida-Matsumoto, L., and Resh, M. D. (2000). Inhibition of protein palmitoylation, raft localization, and T cell signaling by 2-bromopalmitate and polyunsaturated fatty acids. J. Biol. Chem. *275*, 261–270.

Yuste, R., and Bonhoeffer, T. (2004). Genesis of dendritic spines: insights from ultrastructural and imaging studies. Nat. Rev. Neurosci. *5*, 24–34.

Ziv, N. E., and Smith, S. J. (1996). Evidence for a role of dendritic filopodia in synaptogenesis and spine formation. Neuron *17*, 91–102.

Zoghbi, H. Y. (2003). Postnatal neurodevelopmental disorders: meeting at the synapse? Science *302*, 826–830.

Zuo, Y., Lin, A., Chang, P., and Gan, W. B. (2005a). Development of long-term dendritic spine stability in diverse regions of cerebral cortex. Neuron *46*, 181–189.

Zuo, Y., Yang, G., Kwon, E., and Gan, W. B. (2005b). Long-term sensory deprivation prevents dendritic spine loss in primary somatosensory cortex. Nature *436*, 261–265.